

Article

# Enabling Multi-Material Structures of Co-Based Superalloy Using Laser Directed Energy Deposition Additive Manufacturing

Beytullah Aydogan and Himanshu Sahasrabudhe \*

Laboratory for Advanced Manufacturing Processes (LAMP), Department of Mechanical Engineering, Michigan State University, East Lansing, MI 48824, USA; aydoganb@msu.edu

\* Correspondence: sahasra1@egr.msu.edu

**Abstract:** Cobalt superalloys such as Triballoys are widely used in environments that involve high temperatures, corrosion, and wear degradation. Additive manufacturing (AM) processes have been investigated for fabricating Co-based alloys due to design flexibility and efficient materials usage. AM processes are suitable for reducing the manufacturing steps and subsequently reducing manufacturing costs by incorporating multi-materials. Laser directed energy deposition (laser DED) is a suitable AM process for fabricating Co-based alloys. T800 is one of the commercially available Triballoys that is strengthened through Laves phases and of interest to diverse engineering fields. However, the high content of the Laves phase makes the alloy prone to brittle fracture. In this study, a Ni-20%Cr alloy was used to improve the fabricability of the T800 alloy via laser DED. Different mixture compositions (20%, 30%, 40% NiCr by weight) were investigated. The multi-material T800 + NiCr alloys were heat treated at two different temperatures. These alloy chemistries were characterized for their microstructural, phase, and mechanical properties in the as-fabricated and heat-treated conditions. SEM and XRD characterization indicated the stabilization of ductile phases and homogenization of the Laves phases after laser DED fabrication and heat treatment. In conclusion, the NiCr addition improved the fabricability and structural integrity of the T800 alloy.

**Keywords:** additive manufacturing; co-based superalloys; multi-material structures; microstructure; phase characterization



**Citation:** Aydogan, B.; Sahasrabudhe, H. Enabling Multi-Material Structures of Co-Based Superalloy Using Laser Directed Energy Deposition Additive Manufacturing. *Metals* **2021**, *11*, 1717. <https://doi.org/10.3390/met11111717>

Academic Editors: Marco Mandolini, Paolo Cicconi and Patrick Pradel

Received: 24 September 2021

Accepted: 22 October 2021

Published: 27 October 2021

**Publisher's Note:** MDPI stays neutral with regard to jurisdictional claims in published maps and institutional affiliations.



**Copyright:** © 2021 by the authors. Licensee MDPI, Basel, Switzerland. This article is an open access article distributed under the terms and conditions of the Creative Commons Attribution (CC BY) license (<https://creativecommons.org/licenses/by/4.0/>).

## 1. Introduction

Cobalt-based alloys have been utilized widely as protective materials due to their resistance to corrosion and wear [1,2]. Cobalt alloys can be categorized into three types: high-carbon wear resistant alloys, low-carbon high temperature resistant alloys, and low-carbon corrosion and wear resistant alloys [2]. High-carbon wear resistant alloys such as the Stellite 720 alloy are used in biomedical devices such as load bearing implant components [3]. Low-carbon cobalt alloys such as the Stellite 21 alloy are used in applications where high temperatures and high stresses are experienced such as hot stamping dies in manufacturing [4,5]. Lastly, low-carbon corrosion and wear resistance alloys such as Triballoys (registered trademark of Deloro Stellite Company, Koblenz, Germany) find applications in gas turbine components such as blades [6]. These alloys are also known as Laves-phase hardened alloys [2], and are widely used in environments with a wide operating temperature range from 800 °C to over 1000 °C [7,8]. These cobalt-based superalloys are extensively used as protective layers against galling on components under elevated temperatures, and where lubrication is not feasible [9]. However, the fabrication of alloys such as the Triballoys is challenging. Ductility and impact strength are significantly limited in these alloys [2]. Moreover, it is very difficult to attain crack-free structures on large areas.

In recent years, additive manufacturing (AM) was used in many engineering applications such as aerospace, molding, and space due to having advantages over conventional

manufacturing techniques [10,11]. Moreover, AM processes are utilized for fabricating cobalt-based superalloys [4,12–14] due to design flexibility and efficient material usage. Powder bed fusion (PBF) is one of the metal AM techniques that is capable of fabricating complex geometries in a near single step with minimum post processing [12,13,15,16]. The other popular AM technique is laser directed energy deposition (laser DED), which is especially noted for its high volume, rapid fabrication capability. Laser DED is also capable of performing maintenance, refurbishment, or overhaul (MRO) operations on existing structures [17–21]. When used in such configurations, the laser DED AM process can enhance an existing component with the existing material or a new material and subsequently can lead to a lesser wastage of legacy components. The laser DED process was also recently utilized in a novel hybrid mode where additive fabrication and the subtractive machining of components can be performed in the same machine-tool platform. AM processes are also beneficial for reducing the manufacturing steps, subsequently leading to reduced manufacturing costs. Judicious use of materials and manufacturing resources can also be achieved by fabricating multi-material structures. Many engineering structures can be simplified by utilizing multiple materials beyond the limitations set by conventional manufacturing processes. Multi-material structures provide multi-functionality to a component by tailoring the material properties specific to the application. The fabrication of multi-material structures via PBF processes is limited as the processes are restricted to a single material or single mixture of the materials [22,23]. However, the DED processes such as laser DED AM are capable of fabricating multi-material structures with considerable flexibility by using multiple powder feeder systems.

Multi-material and multi-functional structures enabled via AM processes are widely investigated at present, with various metallic or metal-ceramic materials [24–33]. The laser DED AM process uses focused laser energy to melt a steady stream of metallic or metal-ceramic mixture powder. The powdered feedstock material absorbs the laser energy and instantly generates a small melt pool. During fabrication, this melt pool solidifies rapidly. However, the rapid cooling process favors the formation of metastable phases and leads to thermal residual stresses. To fabricate a 3D structure without defects associated with metastable phases and residual stresses such as crack, the feedstock materials must withstand rapid cooling [34–36]. Hence, fabrication of the aforementioned Triballoys is challenging with the laser DED process. The varying proportion of the Laves phases in the microstructure favors the high hardness and wear resistance properties of Triballoys, such as the T800 alloy which contains high proportions of Laves phases. When the Laves phases are evenly dispersed in the matrix at a volume proportion of 40% to 60%, the resultant T800 alloy structure exhibits high wear resistance [1,9,37–39]. However, the high proportion of Laves phases makes the component highly sensitive to brittle fracture, especially when combined with rapidly solidifying manufacturing processes such as the laser DED AM process. Researchers have tried different techniques to mitigate the problems associated with such materials. One solution involves preheating the substrate materials on which the high-performance alloy is to be deposited. Hence, the rapid cooling of the melt pool is suppressed. The T800 alloy can be deposited up to a 5 mm thickness with the laser DED system by preheating the base plate to 500 °C [40]. Keshavarz et al. used the preheating method for welding a T800 alloy and to mitigate the heat-affected-zone liquation cracking by heating over 900 °C [41]. This approach may be suitable for small components where preheating the substrate alleviates rapid cooling through conductive heat transfer but would not work for larger components where the conductive heat transfer is diminished with increasing the thickness of the component. The other approach is to stabilize the rapidly solidified phases by promoting ductile phases. This can be achieved by the diffusion of elements from the substrate materials. Tobar et al. found more than 10% Fe dilution from substrate materials and significant changes to the microstructures of the T800 alloy [8]. However, Fe dilution did not improve structural integrity as the cracks associated with thermal shocks were observed [8]. The present study addresses this technological demand for structurally sound and additively manufactured Co-based alloys such as T800.

In the study, a mixed feedstock powder of the T800 alloy and Ni-20%Cr alloy was processed using the laser DED AM process on a stainless steel 304 substrate. Different mixture compositions (20%, 30%, 40% NiCr in T800 by weight) were investigated. Furthermore, the laser DED fabricated structures were heat treated. These mixtures were characterized for their microstructural, phase, and mechanical properties in the as-fabricated and heat-treated conditions. The NiCr addition improved the laser processability and the structural integrity of the T800 alloy with the trade-off of mechanical properties such as hardness. A 3D component fabrication strategy is proposed based on the results that utilizes the T800 + NiCr alloy chemistries and intermediate heat treatment of the laser fabricated materials.

## 2. Materials and Methods

### 2.1. Laser DED Fabrication of T800 + NiCr Alloy

Laser DED is one of the DED additive manufacturing techniques that uses a laser to melt metal powders to build 3D objects [42]. Three-dimensional objects are designed using a CAD software. A proprietary software then deconstructs the CAD design in the horizontal plane into layers. Each layer consists of raster scans which are essentially toolpaths on the XY plane that the CNC controller follows to deposit the feedstock material powder and focus the energy from the laser source simultaneously. The powder is carried in a pressurized stream of argon inert gas and blown into the focal path of the laser using four sharp delivery nozzles. The laser beam and powder meet on the deposition head, and the material melts rapidly. The CNC controller moves the laser spot, and the melted material rapidly solidifies. The laser DED process is shown in Figure 1. In the present study, coupons from the T800 and NiCr alloy mixtures were fabricated in an inert environment using a custom-built laser DED AM equipment at Michigan State University. This laser DED equipment consists of a LENS Print Engine (Optomec Inc., Albuquerque, NM, USA) and 1000W fiber laser with a wavelength of  $1070 \pm 10$  nm (IPG Photonics, Oxford, MA, USA) and an argon gas filled inert enclosure (Inert Corporation, Amesbury, MA, USA). T800 and NiCr alloy powders (particle size 44–150  $\mu\text{m}$ , Oerlikon Metco (US) Inc., Plymouth, MI, USA) were used. During the printing process, the oxygen and moisture level was maintained below 20 ppm. The powders were premixed with weight percentages of: 20%, 30%, and 40% of the NiCr alloy in the T800 alloy. Powders were hand mixed and hand shook for at least 5 min. The compositions of all the processed alloys are shown in Table 1. Ultra-high purity argon gas was used to carry powder into the deposition head with a flow rate of 4 lpm. The center purge flow rate maintained 22 lpm during fabrication. Coupons were fabricated at a laser power varying from 500 to 600 W, and the laser beam's spot size was maintained at 900  $\mu\text{m}$ . This led to a power density of 785–940  $\text{MW}/\text{m}^2$ . The fabrication parameter is given in Table 2. All coupons were fabricated with the parameters of a 0.30 mm layer thickness, 0.46 mm hatch spacing, and 0–90 raster scan angle. Based on our previous experiments with T800, NiCr, and such other Ni- and Co-based alloys, these parameters were found to be satisfactory for a fabricability test, and a specific investigation into processing parameters for these alloys, or for their heat treatment, was avoided. The fabricated coupons had dimensions of 19 mm  $\times$  19 mm and a thickness of approximately 6 mm. Samples were fabricated on a 6 mm thick Stainless steel 304 (SS304) substrate. An air furnace (MTI Corporation, Richmond, CA, USA) was utilized for heat treatment. Two different heat treatments were applied: one at 400  $^{\circ}\text{C}$  and the other at 980  $^{\circ}\text{C}$ , both with a 60–90 min soaking time, followed by furnace cooling.

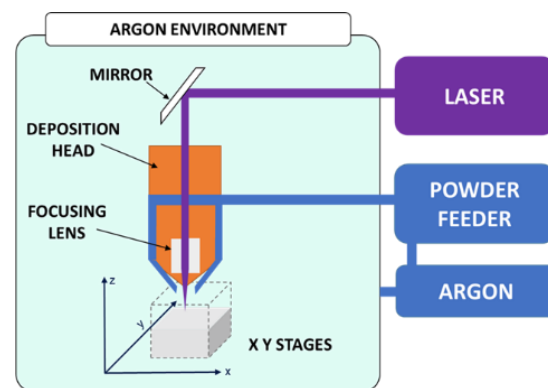


**Figure 1.** Laser DED AM process schematic.

**Table 1.** Chemical composition of T800 and NiCr alloy powders and their mixtures by weight.

	Co	Cr	Mo	Ni	Si	Fe
T800	50.30	17.54	28.51	0.17	3.38	0.05
Ni-20Cr	0.00	19.00	0.00	78.00	1.00	1.00
T800 + %20 NiCr	40.24	17.83	22.81	15.74	2.90	0.24
T800 + %30 NiCr	35.21	17.98	19.96	23.52	2.67	0.34
T800 + %40 NiCr	30.18	18.12	17.11	31.30	2.43	0.43

**Table 2.** Fabrication parameters of T800 and NiCr mixtures by weight.

	Power (W)	Powder Flow Rate (g/min)	Feed Rate (mm/s)
T800	500	8	27.9
T800 + %20 NiCr	600	6	21.2
T800 + %30 NiCr	600	7.6	21.2
T800 + %40 NiCr	600	7.6	25.4

## 2.2. Microstructure, Phase, and Mechanical Characterization

The laser DED fabricated coupons were sectioned using a high-speed abrasive cutoff saw (Presi Mecatone T260, Eybens, France). The size of the sectioned specimens was approximately a 12 mm × 12 mm square section with the SS304 substrate plate attached. An epoxy compound was used to mount specimens before grinding and polishing. All mounted specimens were wet ground from 240 grit to 1200 grit with silicon carbide (SiC) papers and fine polished with a 0.06 μm colloidal silica solution. Specimens were cleaned with an ultrasonic cleaner (SharperTEK XP PRO, Pontiac, MI, USA). A mirror-like finish was verified with an optical microscope. A field emission scanning electron (SEM) microscope (JEOL 6610LV, Tokyo, Japan) was used for characterization with 15 kV operating voltage. An EDS detector (Oxford Instruments X-MAX detector, Abingdon, UK) used for chemical characterization. The phase analysis was performed using the X-ray diffraction (XRD) technique (Rigaku Smartlab, Tokyo, Japan) in the 2θ range of 20° to 100° with a 0.05° step size and Cu Kβ filter at 40 kV. The Vickers microhardness tester (Phase II, Upper Saddle River, NJ, USA) was used for hardness tests with a 15 s dwell time and 100 g fixed load. Four measurements were collected from each polished specimen.

## 3. Results

Four different compositions: 100% T800, T800 + 20% NiCr, T800 + 30% NiCr, and T800 + 40% NiCr were processed using the laser DED technique. A post processing step included heat treatment at two different temperatures. The structural integrity, microstructural features, and phases were characterized using SEM, SEM-EDS, and XRD techniques.

### 3.1. As Processed T800 + NiCr Alloy

A 100% T800 alloy showed extensive cracking and delamination defects after the laser DED process. Cracks were visible during laser DED fabrication of the alloy, and it was not possible to continue depositing any more material once such defects were visible, as the structure would have poor structural integrity. Therefore, for the 100% T800 alloy, the laser DED fabricated coupons only consisted of one layer of deposited material. Cracks and delamination defects were found to decrease as the NiCr content in the T800 alloy was increased during laser processing. Specifically, T800 + 20% NiCr showed fewer cracks than the 100% T800 alloy, and as the content of NiCr was increased to 40% in the mixtures, cracks were no longer visible to the unaided eye during or after deposition. However, the T800 + 20% NiCr and T800 + 30% NiCr compositions still showed hairline cracks when they were sectioned using a cut-off saw. The T800 + 40% NiCr alloy mixture showed no cracks during deposition, after deposition, or even after sectioning using any common laboratory techniques such as cut-off sawing. These results can be observed in Figure 2a–c.

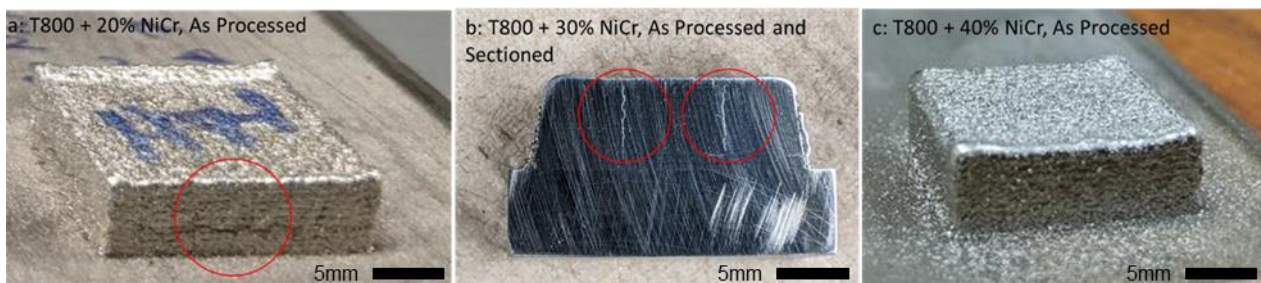


**Figure 2.** Structural integrity of T800 + NiCr alloy, as processed state. (a) Cracks seen after fabrication of T800 + 20% NiCr alloy; (b) Cracks only visible after sectioning in the T800 + 30% NiCr alloy; and (c) No structural defects in the T800 + 40% NiCr alloy. Each coupon is approximately 19 mm × 19 mm × 6 mm size as fabricated.

Figure 3 shows the SEM acquired microstructure of the laser DED processed T800 alloy with a varying amount of the NiCr alloy with 0%, 20%, and 40% by weight. The 100% T800 alloy showed a non-homogeneous microstructure with fine Laves phases distinctly visible after laser DED processing of the alloy powder. As the NiCr content was increased, the microstructure got coarser and more homogeneous, as seen in Figure 3b,c. Finally, the T800 alloy with a 40% NiCr addition showed a cellular microstructure with striated and interconnected Laves phases.

The XRD analysis on all the chemistries explored using the laser DED process revealed phase stabilization in the T800 alloy with an increasing NiCr alloy addition. Specifically, the 100% T800 alloy showed the presence of  $\text{Co}_3\text{Mo}_3\text{Si}$ , along with  $\text{Co}(\text{Cr})$  and  $\text{Co}_2\text{MoCr}$  phases, as seen in Figure 4. As the NiCr alloy content was increased in the laser processed feedstock powder, the  $\text{Co}_3\text{Mo}_3\text{Si}$  phase decreased, along with a parallel increase in the Ni containing  $\text{Co}(\text{CrNi})$  phases.

The segregation of alloying elements such as Mo and Ni was also common in the as processed 100% T800, in the T800 + 20% NiCr, and to a lesser extent in the T800 + 30% NiCr alloys. An example of such segregated Mo-rich regions is shown in the EDS analysis in Figure 5. There were no such regions in the T800 + 40% NiCr alloy, and as aforementioned, the microstructure was more uniform.

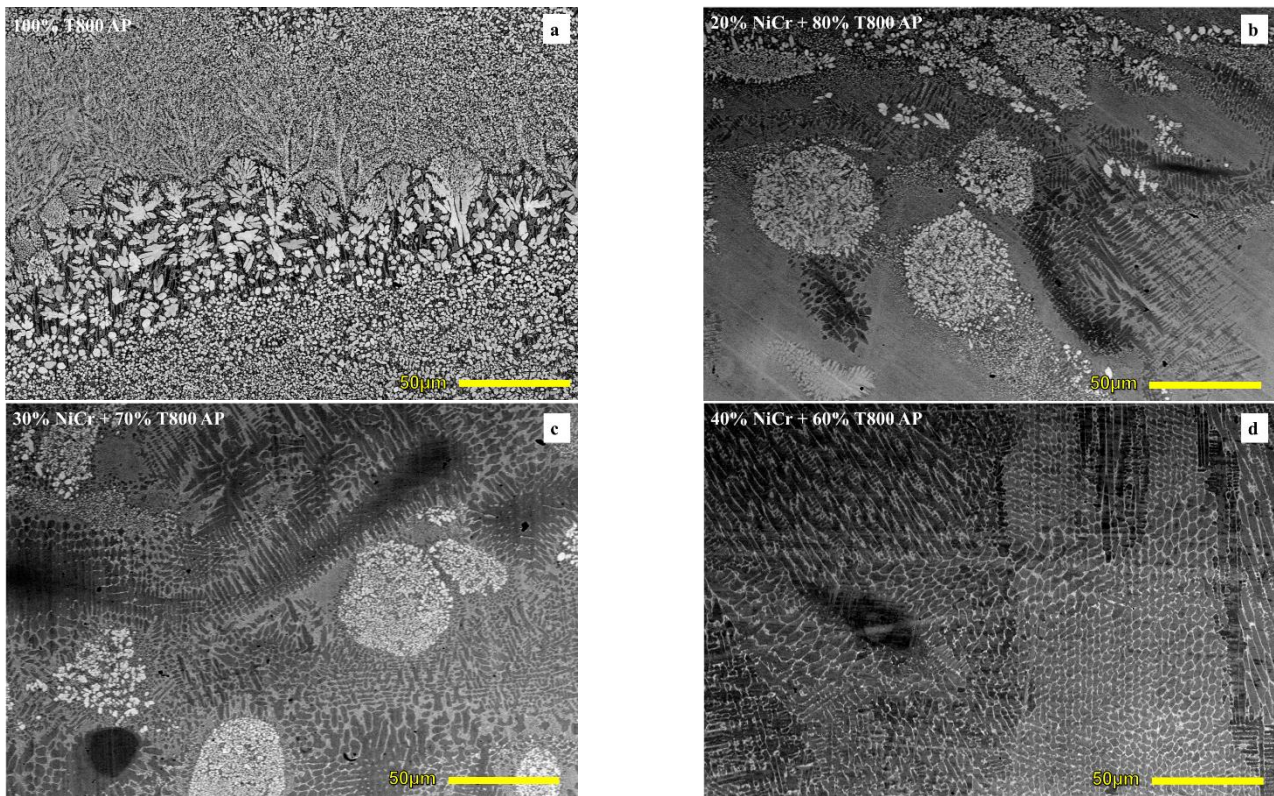


**Figure 3.** SEM microstructure results of as processed (AP) samples. (a) 100% T800, (b) T800 + 20% NiCr, (c) T800 + 30% NiCr, and (d) T800 + 40% NiCr.

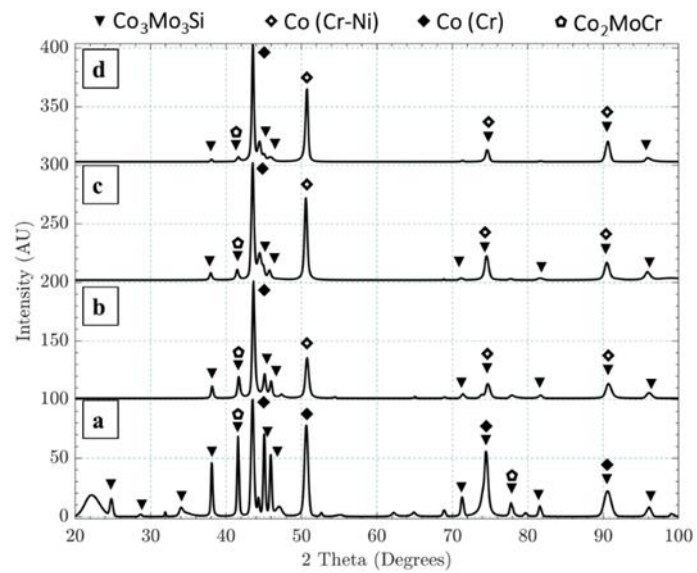


**Figure 4.** XRD results of as processed samples. (a) 100% T800, (b) T800 + 20% NiCr, (c) T800 + 30% NiCr, and (d) T800 + 40% NiCr.

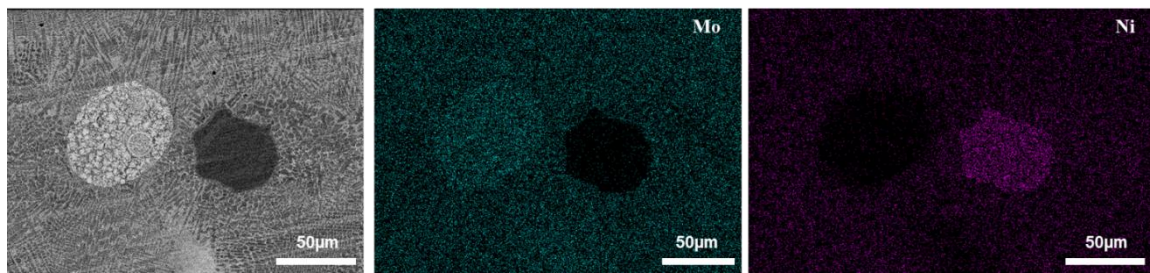


**Figure 5.** EDS elemental map of Nickel and Molybdenum accumulations in the as processed (AP) T800 + 20% NiCr alloy.

### 3.2. Heat Treatment of Laser DED Fabricated T800 + NiCr Alloy

Heat treatment was applied to the T800 + NiCr alloy mixtures to alleviate the microstructural segregation and residual stresses after laser DED fabrication. In the heat treatment experiments, the 100% T800 alloy was not used since the laser DED fabricated alloy showed extensive cracking failure and was not possible to fabricate for more than one or two laser deposited layers. The T800 + 20% NiCr, T800 + 30% NiCr, and T800 + 40% NiCr alloys were all heat treated at 400 °C and 980 °C. The SEM acquired microstructures of these heat treatment experiments are shown in Figure 6. SEM imaging revealed that heat treatment led to a relatively more uniform microstructure as compared to the as processed microstructures from Figure 3. Grain coarsening was more distinctly visible in the heat treated T800 + 20% NiCr and T800 + 30% NiCr alloys. The T800 + 40% NiCr alloy showed no significant changes after heat treatment, and no grain coarsening was observed.

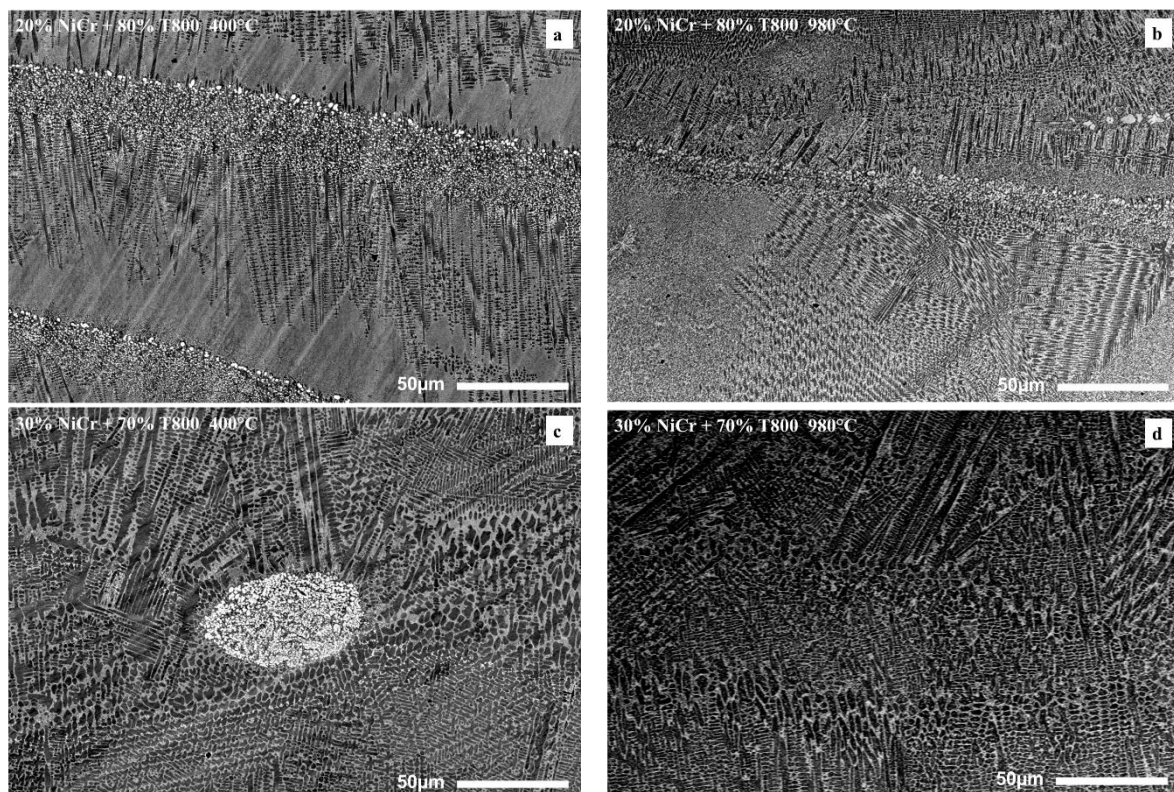


**Figure 6.** Cont.

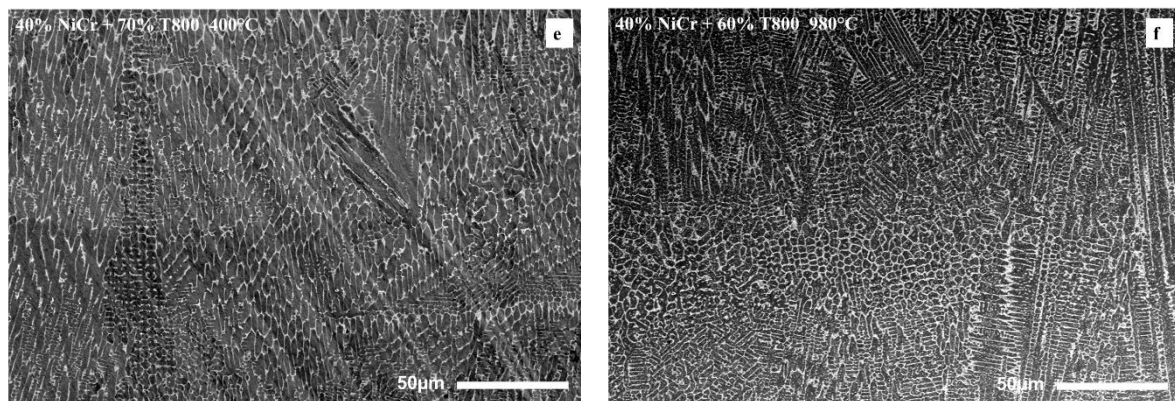


**Figure 6.** SEM microstructure results of heat treated (HT) samples. T800 + 20% NiCr: (a) HT at 400 °C and (b) HT at 980 °C. T800 + 30% NiCr: (c) HT at 400 °C and (d) HT at 980 °C. T800 + 40% NiCr: (e) HT at 400 °C and (f) HT at 980 °C.

The XRD analysis of the T800 + NiCr alloys heat treated at 400 °C showed major differences as compared to the as processed alloys. In the T800 + 30% NiCr and T800 + 40% NiCr alloys, the highest intensity peak shifted from 45° in the as processed state to 51° after heat treatment, as noticed in Figure 7. However, the same trend was not observed after heat treatment at 980 °C. The XRD peaks after heat treatment at 980 °C resembled the peaks from the laser processed alloys, with the major peak once shifting back to approximately 45°.

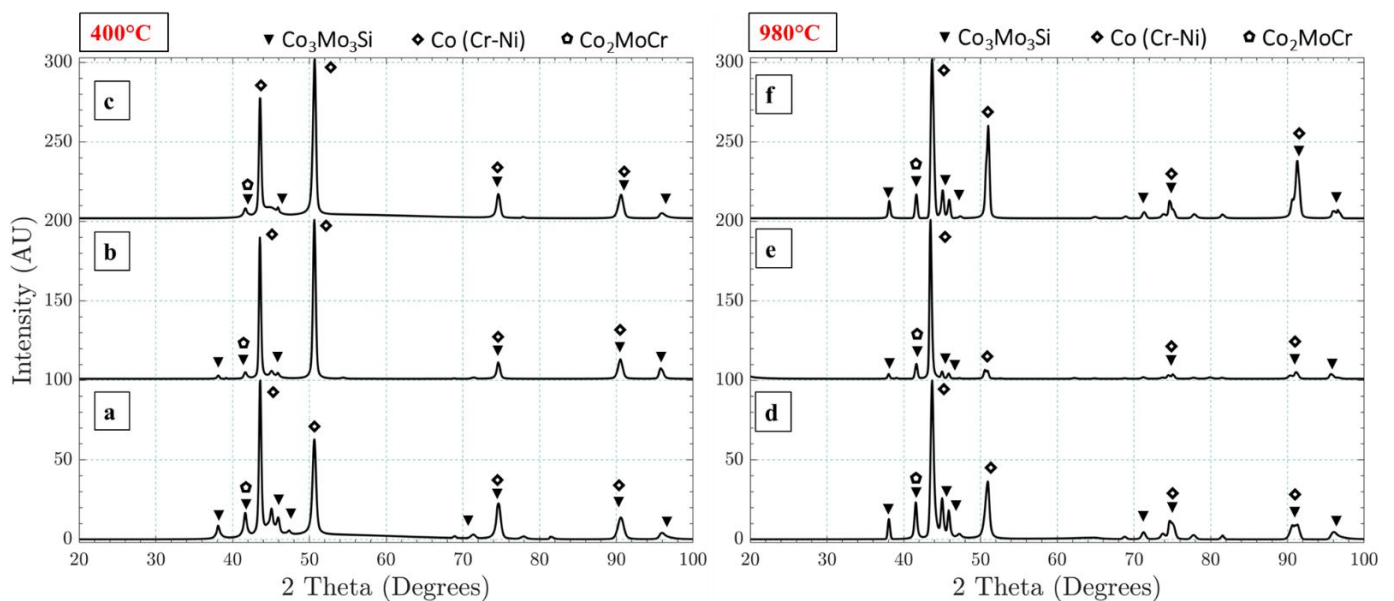


**Figure 7.** XRD results of samples heat treated at 400 °C and 980 °C. (a,d) T800 + 20% NiCr, (b,e) T800 + 30% NiCr, and (c,f) T800 + 40% NiCr.

### 3.3. Microhardness Measurements

Vicker's hardness results for the as processed and heat treated 100% T800 and T800 + NiCr alloy mixtures are graphically presented in Figure 8. The hardness of the samples dropped with the increase in the NiCr weight percentage. The 100% T800 showed the highest hardness of  $949 \pm 110$  HV. This was followed by the T80 + 20% NiCr alloy with the hardness of  $784 \pm 72$  HV in the as processed state,  $681 \pm 36$  HV when heat treated at 400 °C, and  $678 \pm 48$  HV when heat treated at 980 °C. In contrast to the T800 + 20% NiCr alloy, the T800 + 30% alloy showed a different trend. For this composition, higher hardness was obtained with the 980 °C heat treated alloy at  $566 \pm 35$  HV, followed by the as processed alloy at  $508 \pm 100$  HV and then the 400 °C heat treated alloy at  $486 \pm 35$  HV. This trend was also noticed with the T800 + 40% NiCr alloy. For this composition, the 980 °C heat treated

alloy had a hardness of  $480 \pm 6$  HV. The as processed alloy had a hardness of  $430 \pm 14$  HV, whereas the  $400^\circ\text{C}$  heat treated alloy had a hardness of  $400 \pm 5$  HV.

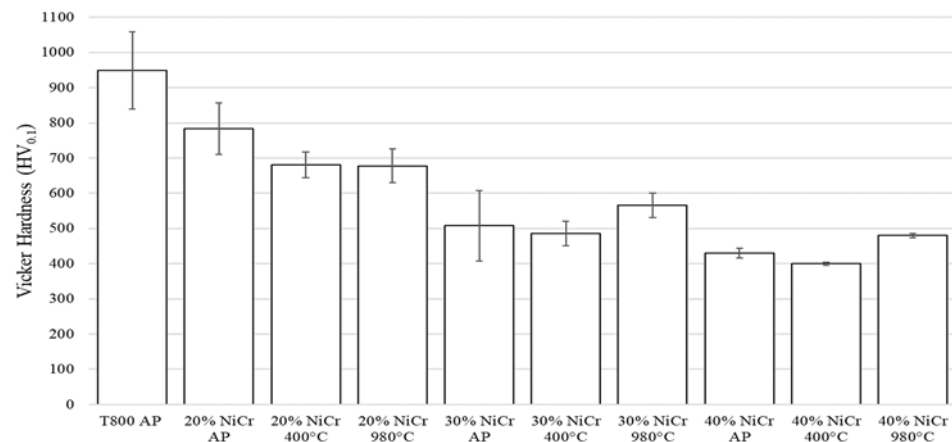


**Figure 8.** Vicker's hardness results of as processed heat treatment ( $400^\circ\text{C}$  and  $980^\circ\text{C}$ ) of T800 and T800 + NiCr alloy chemistries.

#### 4. Discussion

The 100% T800 showed Laves phases as previously reported [8,37,40]. Rapid solidification favors the formation of Laves phases in such alloys, and the laser DED process can have solidification rates of 103 to 105 K/s. However, such cooling rates and Laves phases would also lead to severe thermal shock in the materials, and hence several cracks were seen in the 100% T800 samples in this study. The XRD analysis shows a  $\text{Co}_3\text{Mo}_3\text{Si}$  phase, the main Laves phase, widely present in the laser processed 100% T800 alloy. These Mo-rich Laves phases, however, are also responsible for the high hardness of the alloy. The hardness of this material fluctuated in the range of 850 HV to 1050 HV. This is likely due to the microhardness tester occasionally indenting on a large colony of segregated Laves phases and thus leading to a spike in the material's hardness.

The laser processed T800 + 20% NiCr alloy showed fewer cracks as compared to the 100% T800 alloy. In this alloy chemistry, the NiCr addition increased the strain tolerance caused with rapid solidification. However, the segregation of Laves phase colonies in the microstructure would still generate a high residual stress point in the metallic matrix. These stress points are locations for crack initiation. To counter this by homogenizing the microstructure, intermediate heat treatment was applied to the alloy at  $400^\circ\text{C}$  before the materials were sectioned using a cut-off saw. Cracks were most likely formed before the heat treatment cycle since heat treatment did not yield any positive benefits. However, the homogeneity of the microstructure was improved after heat treatment. Laves phases were still present in the alloy, but large segregated colonies were not observed in the T800 + 20% NiCr alloy. Furthermore,  $980^\circ\text{C}$  improved the homogeneity of the matrix further, but cracks were still present, along with non-segregated Laves phases, similar to the  $400^\circ\text{C}$  heat treatment. This change occurs due to the diffusion of Ni into the matrix during heat treatment. Mo-rich Laves phases were formed in the rapid cooling of individual melt pools for each layer. The effect of the NiCr addition, both with and without heat treatment, was also seen in the hardness values of the T800 + 20% NiCr alloy. In the as processed condition, the hardness of this alloy was approximately 17% lower than the hardness of the laser DED fabricated 100% T800 alloy. After heat treatment, the hardness dropped even further to approximately 30% lower as compared to the 100% T800 alloy, primarily due to the diffusion of Ni in the matrix and the homogenization of the Laves phases throughout the volume of the material. The variations in the hardness values of the T800 + 20% NiCr alloy also reduced after heat treatment. This was also due to the homogenized microstructure after heat treatment, at both  $400^\circ\text{C}$  and  $980^\circ\text{C}$ .

The structural integrity continued to improve with more of the NiCr addition of the T800 alloy during laser DED fabrication. In the T800 + 30% NiCr alloy, the localized Laves phases' colonies in the as processed condition were reduced after heat treatment at 400 °C and 980 °C. As the heat treatment temperature was increased, the hardness also increased in the alloy by approximately 11% as compared to the as processed state, whereas the same alloy chemistry when heat treated at 400 °C showed a decrease in hardness by approximately 4%. This has likely happened due to the high heat treatment temperature of 980 °C which is close to the solutionizing temperature of many Ni-based superalloys such as Inconel 625 and Inconel 718. At this temperature, the softer Ni-rich phases would allow for diffusion of the strengthening Mo-rich phases, thereby improving the hardness. Furthermore, the variation in the hardness also reduced due to a uniform microstructure of the T800 + 30% NiCr alloy after heat treatment. A similar trend in the microstructure and hardness was observed in the T800 + 40% NiCr alloy. This alloy composition did not show any cracking or delamination defects. Overall, this alloy mixture contained more than 31% Ni (by weight) and hence the mixture deviated from a predominantly Co-based alloy to a Co-Ni-based alloy. Due to this, the tendency of the T800 alloy to form brittle Laves phases during laser processing was reduced, and the formation of the relatively ductile Co (CrNi) phases was promoted. The microstructure also did not show any presence of segregated Laves phase colonies that act as stress concentrators in the metallic matrix. Instead, the Mo- and Co-rich phases in this alloy chemistry appeared in the striated morphology that led to a cellular microstructure. The microstructure remained relatively unchanged after heat treatment. However, the relative proportion of different phases changed. Diffusion of the Mo-rich strengthening phases in the Co, Ni, Cr matrix is suspected at a heat treatment temperature of 980 °C, and this is supported by the increase in the hardness of this heat-treated alloy as compared to heat treatment at 400 °C.

Cracking is a very common problem in alloys such as the T800 for laser-based additive manufacturing processes. Rapid cooling and thermal stresses are well known reasons for cracking. Controlling the cooling rate is one of the solutions. However, controlling the cooling rate in a laser DED process is challenging. Base plate heating and/or heating the region of interest was previously found to control the cooling rate so that cracking does not occur [40,41]. Conventionally, thermal residual stresses are eliminated via post heat treatment. Although most of the Co-based alloys are considered as non-heat-treatable alloys, the conventional T800 is widely available in stress relieved conditions. Since the laser DED process causes multiple cooling locations due to layer-based manufacturing, a stress relieving intermediate step becomes vital for the T800 or T800-based alloy chemistries.

Based on the observations of the T800 + NiCr alloy chemistries in the as processed and heat-treated states from the present study, a compositionally graded additive, multi-material additive manufacturing strategy can be envisioned using T800 + NiCr alloys' mixtures and intermediate heat treatment, as depicted in Figure 9. Since cracking gradually reduced with an increasing NiCr content in the T800 alloy, an alloy chemistry containing a 10% NiCr to 20% NiCr alloy in the T800 alloy may be possible to fabricate using highly controlled and optimized processing parameters. However, such an alloy chemistry would have a large thermal mismatch with the underlying Fe-based substrate material. This may be alleviated by using the T800 + 30% NiCr and T800 + 40% NiCr alloy chemistries investigated in the current study. An intermediate heat treatment may also be applied to these two compositionally graded layers to homogenize the microstructure, eliminating Laves phase segregation and subsequently also reducing the residual stress in the laser DED fabricated structure. This step would ensure that the intermediate layers do not crack or delaminate when laser deposition is carried out later on during component fabrication. Since the laser DED process is a freeform technique, this compositionally graded material deposition and intermediate heat treatment approach can be applied to components of various shapes and sizes, and thus benefit new component fabrication as well as overhaul and refurbish existing components with high-performance alloys.

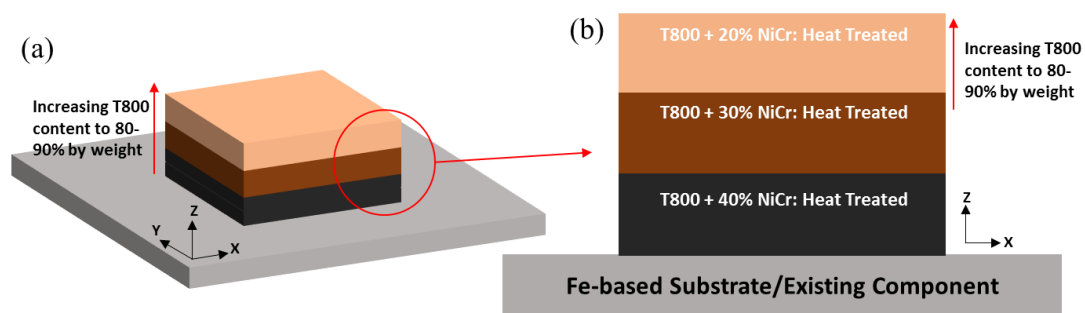


**Figure 9.** Compositionally graded fabrication strategy with T800 + NiCr alloy and intermediate heat treatment. (a) schematic 3D representation and, (b) detail cross section view.

## 5. Conclusions

In this research, different compositions of the T800 and NiCr alloy mixture were investigated for their structural integrity, microstructure, and phase evolution after laser DED fabrication and heat treatment. Based on the results, the main conclusions from this study are as follows.

1. The NiCr addition increased the laser fabricability of the T800 alloy. With the increase in the NiCr, lesser cracks were observed, and eventually, the T800 + 40% NiCr alloy mixture was crack-free.
2. Heat treatment of the T800 + NiCr alloy leads to a homogenized microstructure and more uniform mechanical properties. Heat treatment at 980 °C gave better results compared to heat treatment at 400 °C.
3. Hardness reduced significantly with the NiCr addition. In the T800 + 40% NiCr alloy with 980 °C heat treatment, hardness was reduced by 49% as compared to the laser DED fabricated 100% T800 alloy. However, compared to its as processed state, the T800 + 40% NiCr alloy heat treated at 980 °C had an increase in hardness by 11%.
4. Machining or cutting related failures such as chipping, spalling, and delamination were not observed in the heat treated T800 + NiCr alloys.

**Author Contributions:** Conceptualization, B.A. and H.S.; Methodology, B.A. and H.S.; Investigation, B.A.; Resources, H.S.; Data curation, B.A.; Writing—original draft preparation, B.A.; Writing—review and editing, H.S.; Supervision, H.S. All authors have read and agreed to the published version of the manuscript.

**Funding:** This work was partially supported by the Department of Energy Advanced Research Projects Agency-Energy (ARPA-E) under cooperative agreement DE-AR0001123 with Michigan State University.

**Institutional Review Board Statement:** Not applicable.

**Informed Consent Statement:** Not applicable.

**Data Availability Statement:** The data presented in this study are available on request from the corresponding author. The data are not publicly available as this article is a part of a larger study in this area.

**Acknowledgments:** The authors also acknowledge startup support from Michigan State University. Author Beytullah Aydogan is also grateful for financial support from the Government of the Republic of Turkey. Authors are also grateful to Alexandra Zevalkink for access to XRD analysis facilities. Authors also acknowledge the equipment support from the Center for Advanced Microscopy (CAM) at Michigan State University.

**Conflicts of Interest:** The authors declare no conflict of interest.

## References

1. Halstead, A.; Rawlings, R.D. Structure and Hardness of Co–Mo–Cr–Si Wear Resistant Alloys (Triballoys). *Met. Sci. Heat Treat.* **1984**, *18*, 491–500. [[CrossRef](#)]
2. Davis, J.R. *Nickel, Cobalt, and Their Alloys*; ASM International: Almere, The Netherlands, 2000; ISBN 9780871706850.
3. Hu, P.S.; Liu, R.; Liu, J.; McRae, G. Investigation of Wear and Corrosion of a High-Carbon Stellite Alloy for Hip Implants. *J. Mater. Eng. Perform.* **2014**, *23*, 1223–1230. [[CrossRef](#)]
4. Foster, J.; Cullen, C.; Fitzpatrick, S.; Payne, G.; Hall, L.; Marashi, J. Remanufacture of Hot Forging Tools and Dies Using Laser Metal Deposition with Powder and a Hard-Facing Alloy Stellite 21<sup>®</sup>. *J. Remanuf.* **2019**, *9*, 189–203. [[CrossRef](#)]
5. Yao, J.; Ding, Y.; Liu, R.; Zhang, Q.; Wang, L. Wear and Corrosion Performance of Laser-Clad Low-Carbon High-Molybdenum Stellite Alloys. *Opt. Laser Technol.* **2018**, *107*, 32–45. [[CrossRef](#)]
6. Kathuria, Y.P. Some Aspects of Laser Surface Cladding in the Turbine Industry. *Surf. Coat. Technol.* **2000**, *132*, 262–269. [[CrossRef](#)]
7. Yao, M.X.; Wu, J.B.C.; Yick, S.; Xie, Y.; Liu, R. High Temperature Wear and Corrosion Resistance of a Laves Phase Strengthened Co–Mo–Cr–Si Alloy. *Mater. Sci. Eng. A* **2006**, *435–436*, 78–83. [[CrossRef](#)]
8. Tobar, M.J.; Amado, J.M.; Álvarez, C.; García, A.; Varela, A.; Yáñez, A. Characteristics of Tribaloy T-800 and T-900 Coatings on Steel Substrates by Laser Cladding. *Surf. Coat. Technol.* **2008**, *202*, 2297–2301. [[CrossRef](#)]
9. Cameron, C.B.; Ferriss, D.P. Tribaloy Intermetallic Materials: New Wear- and Corrosion-Resistant Alloys. *Anti-Corros. Methods Mater.* **1975**, *39*, 88. [[CrossRef](#)]
10. Gibson, I.; Rosen, D.; Stucker, B.; Khorasani, M. *Additive Manufacturing Technologies*; Springer Nature: Basingstoke, UK, 2020; ISBN 9783030561277.
11. Hussin, R.B.; Sharif, S.B.; Abd Rahim, S.Z.B.; Suhaimi, M.A.B.; Bin Mohd Khushairi, M.T.; Abdellah EL-Hadj, A.; Shuaib, N.A.B. The Potential of Metal Epoxy Composite (MEC) as Hybrid Mold Inserts in Rapid Tooling Application: A Review. *Rapid Prototyp. J.* **2021**, *27*, 1069–1100. [[CrossRef](#)]
12. Hitzler, L.; Alifui-Segbaya, F.; Williams, P.; Heine, B.; Heitzmann, M.; Hall, W.; Merkel, M.; Öchsner, A. Additive Manufacturing of Cobalt-Based Dental Alloys: Analysis of Microstructure and Physicomechanical Properties. *Adv. Mater. Sci. Eng.* **2018**, *2018*, 8213023. [[CrossRef](#)]
13. Kajima, Y.; Takaichi, A.; Kittikundecha, N.; Nakamoto, T.; Kimura, T.; Nomura, N.; Kawasaki, A.; Hanawa, T.; Takahashi, H.; Wakabayashi, N. Effect of Heat-Treatment Temperature on Microstructures and Mechanical Properties of Co–Cr–Mo Alloys Fabricated by Selective Laser Melting. *Mater. Sci. Eng. A* **2018**, *726*, 21–31. [[CrossRef](#)]
14. Chen, J.; Yang, Y.; Wu, S.; Zhang, M.; Mai, S.; Song, C.; Wang, D. Selective Laser Melting Dental CoCr Alloy: Microstructure, Mechanical Properties and Corrosion Resistance. *Rapid Prototyp. J.* **2021**, *27*, 1457–1466. [[CrossRef](#)]
15. Gokuldoss, P.K.; Kolla, S.; Eckert, J. Additive Manufacturing Processes: Selective Laser Melting, Electron Beam Melting and Binder Jetting-Selection Guidelines. *Materials* **2017**, *10*, 672. [[CrossRef](#)]
16. Cunningham, R.; Narra, S.P.; Ozturk, T.; Beuth, J.; Rollett, A.D. Evaluating the Effect of Processing Parameters on Porosity in Electron Beam Melted Ti-6Al-4V via Synchrotron X-ray Microtomography. *JOM* **2016**, *68*, 765–771. [[CrossRef](#)]
17. Nicolaus, M.; Rottwinkel, B.; Alfred, I.; Möhwald, K.; Nölke, C.; Kaieler, S.; Maier, H.J.; Wesling, V. Future Regeneration Processes for High-Pressure Turbine Blades. *CEAS Aeronaut. J.* **2018**, *9*, 85–92. [[CrossRef](#)]
18. Rottwinkel, B.; Nölke, C.; Kaieler, S.; Wesling, V. Crack Repair of Single Crystal Turbine Blades Using Laser Cladding Technology. *Procedia CIRP* **2014**, *22*, 263–267. [[CrossRef](#)]
19. Graf, B.; Gumenyuk, A.; Rethmeier, M. Laser Metal Deposition as Repair Technology for Stainless Steel and Titanium Alloys. *Phys. Procedia* **2012**, *39*, 376–381. [[CrossRef](#)]
20. Bi, G.; Gasser, A. Restoration of Nickel-Base Turbine Blade Knife-Edges with Controlled Laser Aided Additive Manufacturing. *Phys. Procedia* **2011**, *12*, 402–409. [[CrossRef](#)]
21. Liu, Q.; Wang, Y.; Zheng, H.; Tang, K.; Li, H.; Gong, S. TC17 Titanium Alloy Laser Melting Deposition Repair Process and Properties. *Opt. Laser Technol.* **2016**, *82*, 1–9. [[CrossRef](#)]
22. Terrazas, C.A.; Gaytan, S.M.; Rodriguez, E.; Espalin, D.; Murr, L.E.; Medina, F.; Wicker, R.B. Multi-Material Metallic Structure Fabrication Using Electron Beam Melting. *Int. J. Adv. Manuf. Technol.* **2014**, *71*, 33–45. [[CrossRef](#)]
23. Thompson, S.M.; Bian, L.; Shamsaei, N.; Yadollahi, A. An Overview of Direct Laser Deposition for Additive Manufacturing; Part I: Transport Phenomena, Modeling and Diagnostics. *Addit. Manuf.* **2015**, *8*, 36–62. [[CrossRef](#)]
24. Quan, Z.; Wu, A.; Keefe, M.; Qin, X.; Yu, J.; Suhr, J.; Byun, J.-H.; Kim, B.-S.; Chou, T.-W. Additive Manufacturing of Multi-Directional Preforms for Composites: Opportunities and Challenges. *Mater. Today* **2015**, *18*, 503–512. [[CrossRef](#)]
25. Bandyopadhyay, A.; Heer, B. Additive Manufacturing of Multi-Material Structures. *Mater. Sci. Eng. R Rep.* **2018**, *129*, 1–16. [[CrossRef](#)]
26. Zhang, Y.; Sahasrabudhe, H.; Bandyopadhyay, A. Additive Manufacturing of Ti-Si-N Ceramic Coatings on Titanium. *Appl. Surf. Sci.* **2015**, *346*, 428–437. [[CrossRef](#)]
27. Sahasrabudhe, H.; Bandyopadhyay, A. Additive Manufacturing of Reactive In Situ Zr Based Ultra-High Temperature Ceramic Composites. *JOM* **2016**, *68*, 822–830. [[CrossRef](#)]
28. Carroll, B.E.; Otis, R.A.; Borgonia, J.P.; Suh, J.-O.; Dillon, R.P.; Shapiro, A.A.; Hofmann, D.C.; Liu, Z.-K.; Beese, A.M. Functionally Graded Material of 304L Stainless Steel and Inconel 625 Fabricated by Directed Energy Deposition: Characterization and Thermodynamic Modeling. *Acta Mater.* **2016**, *108*, 46–54. [[CrossRef](#)]

29. Feenstra, D.R.; Banerjee, R.; Fraser, H.L.; Huang, A.; Molotnikov, A.; Birbilis, N. Critical Review of the State of the Art in Multi-Material Fabrication via Directed Energy Deposition. *Curr. Opin. Solid State Mater. Sci.* **2021**, *25*, 100924. [[CrossRef](#)]
30. Zuback, J.S.; Palmer, T.A.; DebRoy, T. Additive Manufacturing of Functionally Graded Transition Joints between Ferritic and Austenitic Alloys. *J. Alloys Compd.* **2019**, *770*, 995–1003. [[CrossRef](#)]
31. Shah, K.; Haq, I.u.; Khan, A.; Shah, S.A.; Khan, M.; Pinkerton, A.J. Parametric Study of Development of Inconel-Steel Functionally Graded Materials by Laser Direct Metal Deposition. *Mater. Des.* **2014**, *54*, 531–538. [[CrossRef](#)]
32. Wu, D.; Liang, X.; Li, Q.; Jiang, L. Laser Rapid Manufacturing of Stainless Steel 316L/Inconel718 Functionally Graded Materials: Microstructure Evolution and Mechanical Properties. *Int. J. Opt.* **2011**, *2010*, 802385. [[CrossRef](#)]
33. Onuike, B.; Bandyopadhyay, A. Additive Manufacturing of Inconel 718–Ti6Al4V Bimetallic Structures. *Addit. Manuf.* **2018**, *22*, 844–851. [[CrossRef](#)]
34. Bandyopadhyay, A.; Bose, S. *Additive Manufacturing*; CRC Press: Boca Raton, FL, USA, 2015; ISBN 9781482223606.
35. AlMangour, B. *Additive Manufacturing of Emerging Materials*; Springer: London, UK, 2019; ISBN 9783319917139.
36. *ASTM Standard F3187-16 Standard Guide for Directed Energy Deposition of Metals*; ASTM International: West Conshohocken, PA, USA, 2016.
37. Zhang, Y.-D.; Zhang, C.; Lan, H.; Hou, P.Y.; Yang, Z.-G. Improvement of the Oxidation Resistance of Tribaloy T-800 Alloy by the Additions of Yttrium and Aluminium. *Corros. Sci.* **2011**, *53*, 1035–1043. [[CrossRef](#)]
38. Halstead, A.; Rawlings, R.D. The Fracture Behaviour of Two Co-Mo-Cr-Si Wear Resistant Alloys (“Triballoys”). *J. Mater. Sci.* **1985**, *20*, 1248–1256. [[CrossRef](#)]
39. Halstead, A.; Rawlings, R.D. The Effect of Iron Additions on the Microstructure and Properties of the “Triballoy” Co-Mo-Cr-Si Wear Resistant Alloys. *J. Mater. Sci.* **1985**, *20*, 1693–1704. [[CrossRef](#)]
40. Durejko, T.; Łazińska, M.; Dworecka-Wójcik, J.; Lipiński, S.; Varin, R.A.; Czujko, T. The Tribaloy T-800 Coatings Deposited by Laser Engineered Net Shaping (LENSTM). *Materials* **2019**, *12*, 1366. [[CrossRef](#)] [[PubMed](#)]
41. Keshavarz, M.K.; Gontcharov, A.; Lowden, P.; Brochu, M. A Comparison of Weldability, Structure, and Mechanical Properties of CM64 and Tribaloy T-800 Welds for Hard-Facing of Turbine Blades. *J. Manuf. Sci. Eng.* **2020**, *142*, 101004. [[CrossRef](#)]
42. ISO/ASTM52900-15 Standard Terminology for Additive Manufacturing-General Principles-Terminology. Available online: <https://www.astm.org/Standards/ISOASTM52900.htm> (accessed on 15 October 2021).